Ferroelectric properties of lead zirconate titanate thin films obtained by RF magnetron sputtering near the morphotropic phase boundary

© M.V. Staritsyn[1], M.L. Fedoseev[1], D.A. Kiselev[2], E.Yu. Kaptelov[3], I.P. Pronin[3,¶],
   S.V. Senkevich[3], V.P. Pronin[4]

[1] Central Research Institute of Structural Materials „Prometey" National Research Centre Kurchatov Institute,
St. Petersburg, Russia
[2] National University of Science and Technology „MISiS",
Moscow, Russia
[3] Ioffe Institute,
St. Petersburg, Russia
[4] Herzen State Pedagogical University of Russia
St. Petersburg, Russia

[¶] E-mail: Petrovich@mail.ioffe.ru

An experimental study of the crystal structure and ferroelectric properties of $\langle 110 \rangle$-textured lead zirconate titanate films with a fine variation in their composition (with a change in the elemental ratio of zirconium and titanium atoms within 1.5%) near the morphotropic phase boundary revealed jump-like changes in the pseudocubic lattice parameter, dielectric permittivity and residual polarization. It is assumed that the observed anomalies correspond to a morphotropic transition from a rhombohedral to a mixture of tetragonal and monoclinic phases.

Keywords: fine composition variation, phase state, piezoresponse force microscopy, abnormal dielectric and piezoelectric properties.

1. Introduction

Since 1960s $Pb(Zr_x Ti_{1-x})O_3$ ferroelectric solid solutions of lead zirconate titanate (PZT) are the basic materials for modern piezotechnics [1–3]. Solid solutions of practical importance correspond to morphotropic phase boundary (MPB). This boundary separates rhombohedral (R_{HT}) and tetragonal (T) modifications of ferroelectric phase where electromechanical properties and other important physical parameters achieve the extremely high values, Figure 1, *a* [1].

Recently, microelectromechanical systems (MEMS) with various functionality based on PZT thin films have become increasingly widespread [4–7]. Their performance depends on several factors, such as film composition, elemental heterogeneity on thickness, magnitude and type of mechanical stresses applied from the substrate and sublayers, growth texture orientation, grain size, extrinsic phase inclusions, etc.

Besides, it is important to identify the causes of extreme physical properties at MPB. Initial understanding (Isupov [8,9]) were associated with additional contribution to piezoeffect from the movement of phase boundaries R_{HT}- and T-phases whose coexistence is caused by similarity of their free energies. Further attempts to explain the effect were associated with the approach described in [10,11] for $BaTiO_3$ (both for single crystals and ceramic specimens) whose piezoelectric moduli (and permittivity) increase by several orders with decrease in domain sizes by several

orders into submicrometer region. According to the developed approach, the main contribution to the piezoelectric moduli is made by the domain boundaries (~ 10 nm wide), within which cubic perovskite distortions are minimum.

Another approach was demonstrated in [12–15], where a high-resolution X-ray setup and synchrotron radiation were used for the phase analysis of bulk PZT ceramic samples in the MPB region using high-resolution X-ray and synchrotron radiation equipment. According to this approach, intermediate monoclinic (M) ferroelectric phase located in the narrow concentration range between R_{HT}- and T-phases, Figure 1, *b*, is responsible for electromechanical anomalies. Potential existence of M-phase in the MPB region was reported in several theoretical publications where, according to the calculations, higher electromechanical factors than in R_{HT}- and T-phases [16–19] should have been observed. In accordance with the experimental investigations, M-phase existence area decreases with temperature increasing, and when the temperature is above room temperature, only coexistence of M- and T-phases appears to be stable, Figure 1, *b*. However, though high-precision X-ray equipment is used, no clear interpretation of X-ray diffraction lines was achieved due to the similar type of reflex splitting specific to M-, R_{HT}- mixture and T-phases. In PZT thin films, traces of M-phase were detected in single crystal (epitaxial) layers grown on $SrTiO_3$ single crystall substrates with $\langle 110 \rangle$ type orientation; while no reflex splitting traces were observed on substrates with $\langle 100 \rangle$-
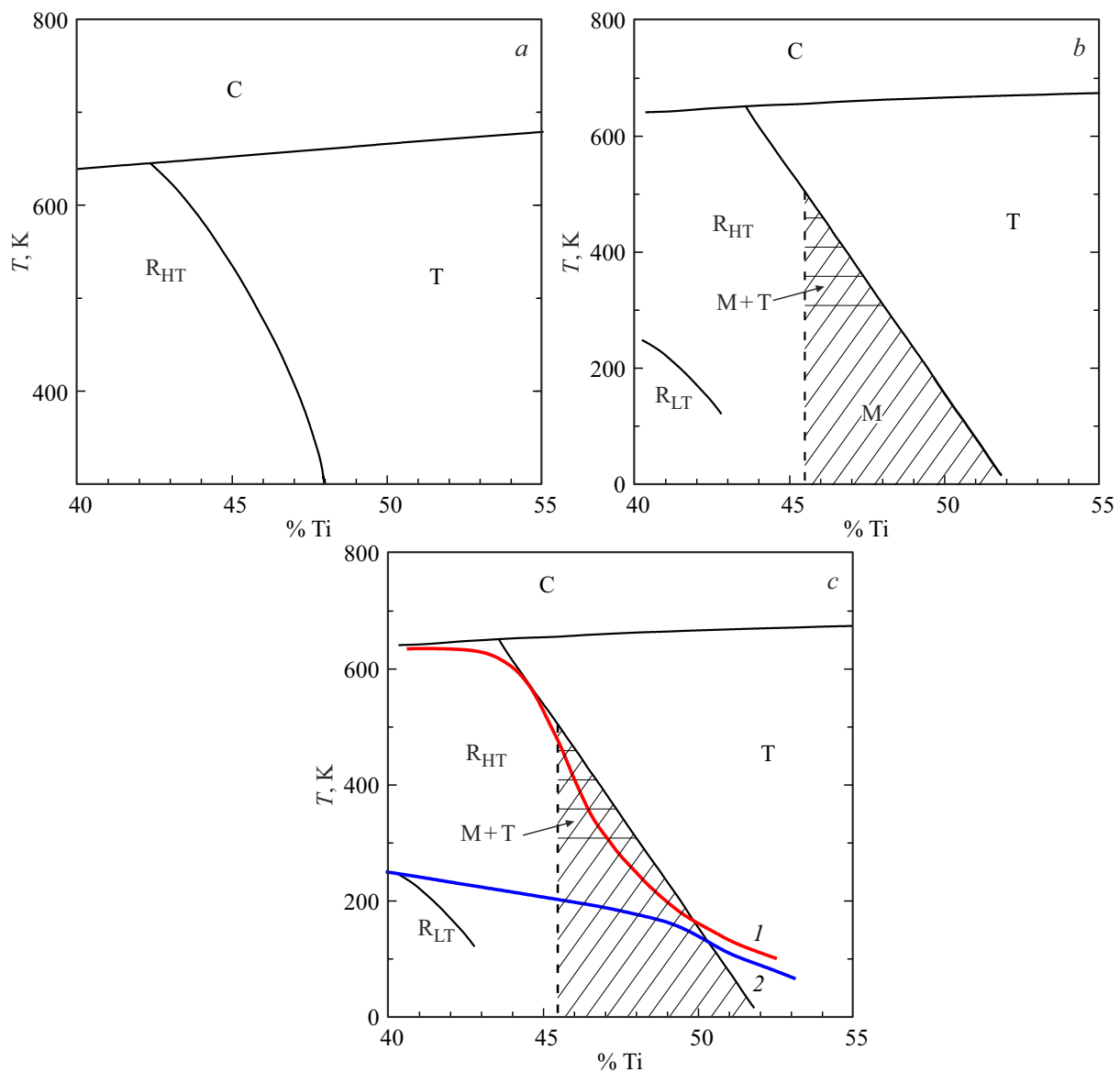
Figure 1. Phase diagram of PZT solid solutions in MPB region according to: *a*) [1], *b*) [12], *c*) [21]. Line *1* in Figure 1, *c* corresponds to MPB, line *2* corresponds to the phase transition temperature associated with octahedra tilting. C is the cubic phase, R_{HT} is the high-temperature rhombohedral phase, R_{LT} is the low-temperature rhombohedral phase, T is the tetragonal phase, M is the monoclinic phase.

and $\langle 111 \rangle$-orientations [20]. For practically important thin polycrystalline (or „ceramic") PZT films which account for the great majority of investigations, existence of M-phase was not reported.

Increasing complexity of the phase diagram in the MPB region is attributed to the proximity of a phase transition caused by oxygen octahedra rotation observed in bulk ceramic specimens, Figure 1, *c* [21–23]. Since this structural transition is below room temperature, it hardly has any influence on the electromechanical properties of piezoelectric ceramics at room temperature and above. However, for thin polycrystalline PZT films where mechanical stresses from the substrate and other sublayers may considerably influence the MPB position and properties due to the difference

in thermal linear expansion coefficients, their influence on the temperature of this transition and its influence on ferroelectric properties cannot be avoided [24,25].

The purpose of this study was to locate morphotropic phase transition in PZT films formed on platinized silicon substrates with fine variation of film composition, and to investigate the features of their ferroelectric behavior.

2. Specimen preparation and study methods

For the purpose of this study, PZT thin films were deposited by radio-frequency magnetron deposition of ce-
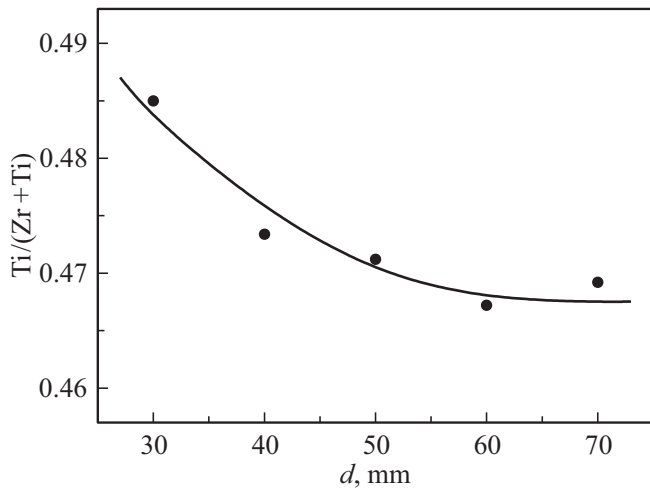
Figure 2. Variation of atomic ratio of titanium and zirconium in deposited thin PZT films with variation of target–substrate distance.

ramic target composed of $PbZr_{0.54}Ti_{0.46}O_3$ on platinized silicon substrates $(Pt|TiO_2|SiO_2|Si)$ with variation of target–substrate distance d within $30-70$ mm. Substrate temperature caused by substrate heating in plasma varied from 90 to 160°C. Deposited layer thickness was 500 nm. By varying the target–substrate distance, fine varying of the deposited film composition (atomic ratio of Ti and Zr) was achieved within Ti/Zr $\sim 48.5/51.5-47.0/53.0$, i.e. by 1.5%, Figure 2 [26,27]. Such variations of complex film composition were associated with the thermalization length difference in gas plasma of atoms which differ in their weight [28,29]. Films were deposited at the same magnetron power and working gas pressure 8 Pa. In order to produce films with the same thickness, deposition time was varied from 1.6 (at 30 mm) to 3.7 h (at 70 mm). The perovskite phase synthesis was followed by furnace annealing at 580°C during 1 h. For electrophysical measurements, platinum contact pads $100 \times 100 \mu$m were formed on free surface of the films.

Composition of films was measured by the electron probe X-ray microanalysis method using Lyra 3 (Tescan) scanning electron microscope equipped by characteristic X-ray radiation energy-dispersive detector (X-Max 50). The probe electron beam energy was equal to 12 keV. The crystalline structure and phase state of films were measured by the X-ray diffraction analysis method (Rigaku Ultima IV). Film surface microstructure images were obtained by atomic force microscopy method. To measure the vertical piezoresponse component, the piezoresponse force microscopy method was used (PFM, Ntegra Prima atomic-force microscope NT-MDT SI, Russia). The measurements were carried out in contact mode with 5 V AC 50 kHz voltage applied to the cantilever. The scanned surface area was $40 \times 40 \mu$m. For dielectric property investigations, an automated package based on LCR meter E7-20 was used.

3. Experimental findings and discussion

According to X-ray diffraction analysis data $(\theta - 2\theta)$, the formed films had a single-phase pseudocubic perovskite structure and prevailing growth $\langle 110 \rangle$-texture (Figure 3).
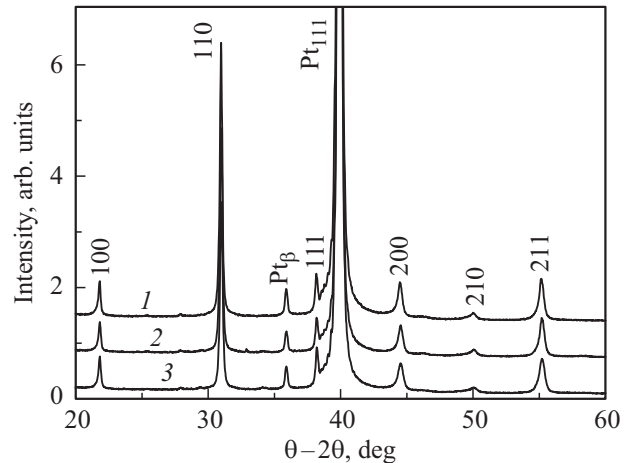

Figure 3. X-ray diffraction spectra $(\theta - 2\theta)$ of PZT perovskite thin films produced by varying the target–substrate distance: *1* — 30, *2* — 50, *3* — 70 mm.
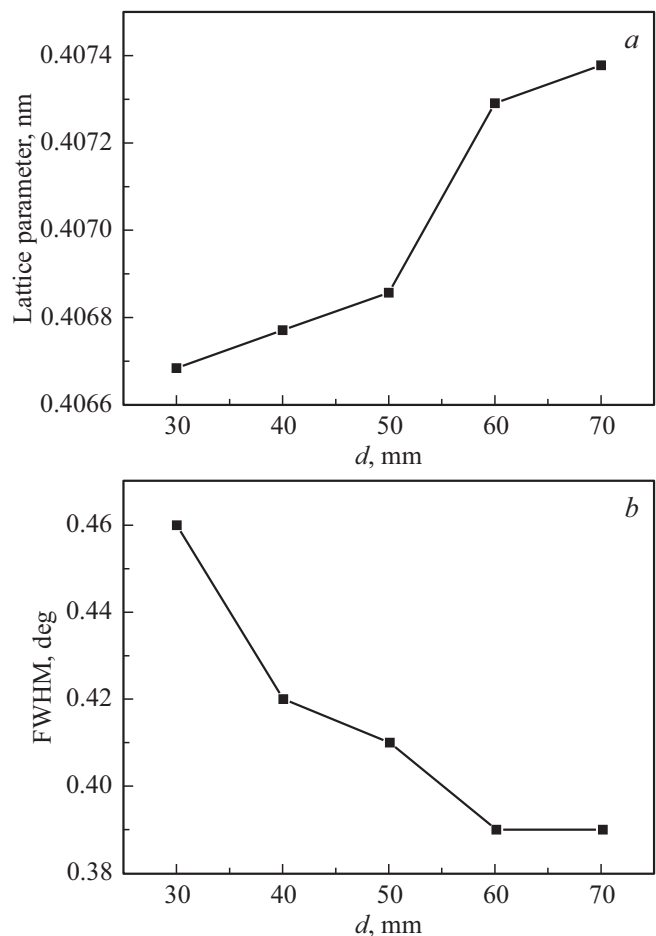

Figure 4. Variation of pseudocubic parameter (a) and half-width of (200)-reflex (b) calculated from PZT film X-ray images.
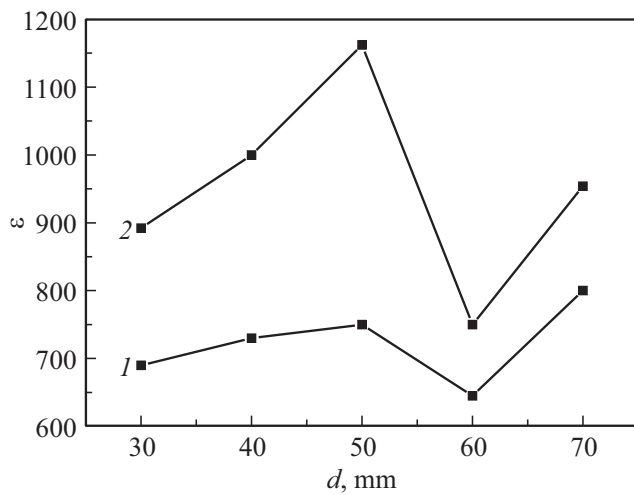
Figure 5. Variation of permittivity values ε (curve *1*) and ε_{max} (curve *2*) measured at room temperature with variation of target–substrate distance. Measurement frequency is 10 kHz.

With growth of Ti atom content (with decrease in target–substrate distance), sharp change in pseudocubic lattice parameter was observed (Figure 4, *a*), which was calculated by the position in the reflex diffraction pattern (200). Such behavior was probably attributed to transformation from R_{HT}-phase to the mixture consisting of M- and T-phases [12–15]. No reflex splitting corresponding these phases was observed, however, with growth of Ti atom content, their half-width (FWHM) increased (Figure 4, *b*). The absence of splitting may be due to the fact that the reflexes were extensively widened. The most probable cause of such widening is nonuniform distribution of Ti and Zr atoms over the thickness, which, as estimated, reached $\sim 3\%$ [26,27].

Figure 5 shows the dielectric permittivity measurements carried out on specimens at room temperature. Curve *1* corresponds to the permittivity at room temperature ε without

application of an external shifting field, and curve *2* corresponds to maximum permittivity values ε_{max} obtained from the voltage-capacitance measurements ($C-V$).

The dependences have a jump in the MPB area, while the permittivity values are still rather high for thin films ($\sim 600-800$ for ε and $\sim 800-1200$ for ε_{max}).

Normal component of the piezoelectric response of the film (signal Mag×Cos) deposited at target–substrate distance equal to 50 mm is shown in Figure 6, *a*. The left part of the central region on the scan is a signal proportional to the residual polarization (P_r^+) achieved by means of positive potential +40 V applied to the free surface of the film, while the right part is the signal (P_r^-) measured after application of −40 V. The image periphery corresponds to the signal from the non-polarized part of the film which means that self-induced polarization is present.

Self-polarization was approximately 1/3 of the residual polarization. Similar signals were received on all test specimens. Figure 6, *b* reflects residual polarization distribution over AB line.

Based on the obtained results, an averaged polarization dependence calculated as $(P_r^+ + P_r^-)/2$ was plotted (Figure 7). This dependence, as the previous figures (Figures 4 and 5), reflects the jump, which also supports the presence of rather sharp (morphotropic) phase boundary.

Thus, by fine variation of PZT film element composition (Ti/Zr atom ratio), the following were observed:

a) sharp increase in pseudocubic lattice parameter with growth of Zr atom content, which is consistent with the phase analysis of epitaxial PZT thin films in the MPB region [30];

b) sharp changes in permittivity and residual polarization which may be associated with the behavior of these parameters in thin films distinguished by growth ⟨110⟩-texture. Similar changes in residual polarization (drop in T-phase area and jump-like increase during transition to R_{HT}-phase) in the MPB region have been observed
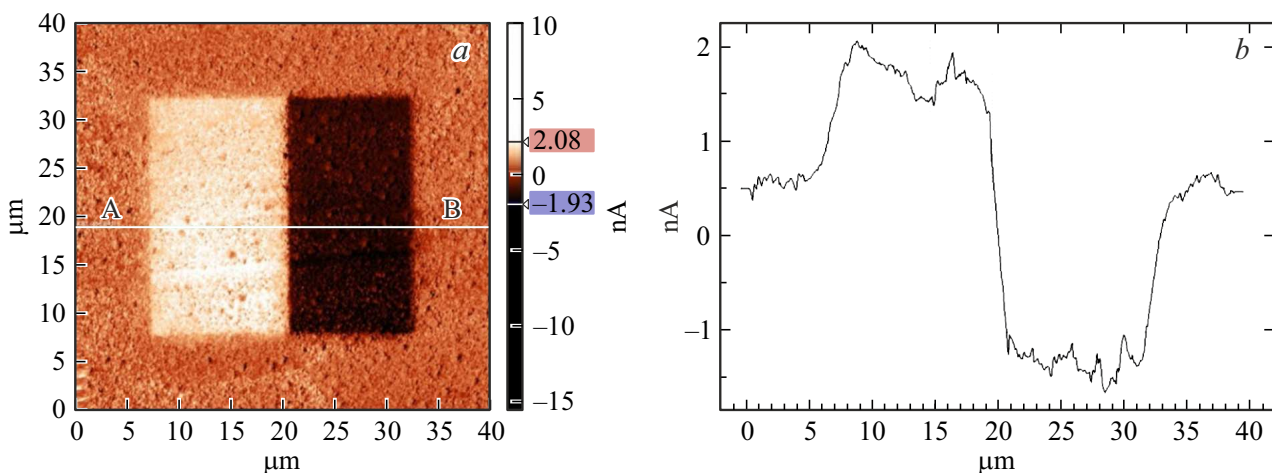

Figure 6. Piezoelectric response of the PZT thin film: *a* — left (P_r^+) and right (P_r^-) parts of the image are polarized with +40 V and −40 V, respectively, *b* — piezoresponse distribution diagram on AB line.
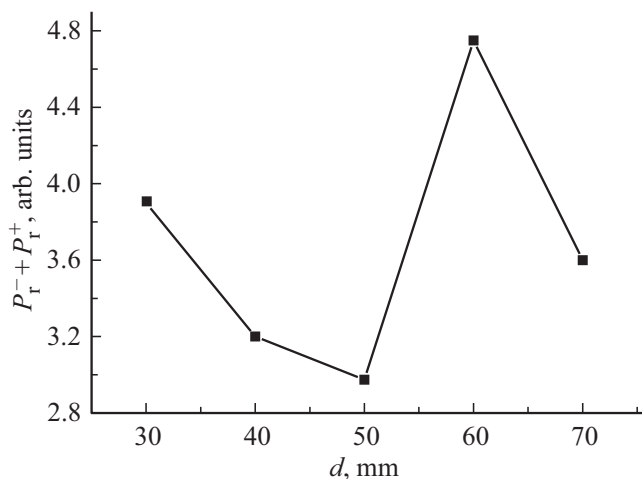
Figure 7. Variation of residual polarization measured on hysteresis loops of PZT films depending on the target–substrate distance.

earlier in $\langle 110 \rangle$-epitaxial PZT films [31]. Abnormal changes in permittivity generally also correlate with the findings herein.

4. Conclusions

1. Review of the available literature and the findings herein prove that with growth of titanium atom content in the MPB region, variation of structure and physical properties of thin films may be attributed to the phase transformation from a rhombohedral phase (R_{HT}) to a phase state containing monoclinic and tetragonal phases (M+T). This phase transition whose precise position was not defined before is marked by vertical dashed line in Figure 1, *b*.

2. Stability of M-phase in $\langle 110 \rangle$-textured thin films may be attributed to the anisotropy of two-dimensional tensile stresses applied to the thin film from the silicon substrate [23,24] similar to the case with $\langle 110 \rangle$-epitaxial PZT thin films grown on strontium titanate single crystals [20]. This assumption regarding the mechanical stress anisotropy in polycrystalline PZT thin films requires a separate study of their calculations.

Conflict of interest

The authors declare that they have no conflict of interest.

References

[1] B. Jaffe, W. Cook, H. Jaffe. Piezoelectric ceramics. London; N.Y.: Academic Press, (1971). 328 p.

[2] Y. Xu. Ferroelectric materials and their applications. North-Holland, Amsterdam, London, N.Y., Tokyo (1991). 391 p.

[3] A.V. Gorish, V.P. Dudkevich, M.F. Kupriyanov, A.E. Panich, A.V. Turik. Piezoelektricheskoe priborostroenie. T. 1. Fizika segnetoelektricheskoi keramiki. IPRZhR, M. (1999). 368 p. (in Russian).

[4] D.L. Polla. Microelectron. Eng. **29**, *1−4*, 51 (1995).

[5] S. Trolier-McKinstry, P. Muralt. J. Electroceram. **12**, *1−2*, 7 (2004).

[6] N. Balke, I. Bdikin, S.V. Kalinin, A.L. Kholkin. J. Am. Ceram. Soc. **92**, *8*, 1629 (2009).

[7] L. Song, S. Glinsek, E. Defay. Appl. Phys. Rev. **8**, *4*, 041315 (2021).

[8] V.A. Isupov. FTT **26**, *1*, 243 (1984). (in Russian).

[9] V.A. Isupov. Phys. Solid State **43**, *12*, 2262 (2001).

[10] S. Wada, K. Yako, K. Yokoo, H. Kakemoto, T. Tsurumi. Ferroelectrics **334**, *1*, 17 (2006).

[11] S. Wada, T. Muraishi, K. Yokoh, K. Yako, H. Kamemoto, T. Tsurumi. Ferroelectrics **355**, *1*, 37 (2007).

[12] B. Noheda, D.E. Cox, G. Shirane, J.A. Gonzalo, L.E. Cross, S.-E. Park. Appl. Phys. Lett. **74**, *14*, 2059 (1999).

[13] B. Noheda, D.E. Cox, G. Shirane, R. Guo, B. Jones, L.E. Cross. Phys. Rev. B **63**, *1*, 014103 (2000).

[14] D.E. Cox, B. Noheda, G. Shirane. Phys. Rev. B **71**, *13*, 134110 (2005).

[15] B. Noheda, D.E. Cox. Phase Transitions **79**, *1−2*, 5 (2006).

[16] Yu.M. Gufan, V.P. Sakhnenko. JETP **42**, *4*, 728 (1975).

[17] D. Vanderbilt, M.H. Cohen. Phys. Rev. B **63**, *9*, 094108 (2001).

[18] I.A. Sergeenko, Yu.M. Gufan, S. Urazhdin. Phys. Rev. B **65**, *14*, 144104 (2002).

[19] X.Q. Ke, D. Wang, X. Ren, Y. Wang. Phys. Rev. B **88**, *21*, 214105 (2013).

[20] L. Yan, J. Li, H. Cao, D. Viehland. Appl. Phys. Lett. **89**, 26, 262905 (2006).

[21] D.I. Woodward, J. Knudsen, I.M. Reaney. Phys. Rev. B **72**, *10*, 104110 (2005).

[22] F. Cordero. Materials **8**, *12*, 8195 (2015).

[23] K. Yan, S. Ren, M.X. Fang, X.-B. Ren. Acta Materialia **134**, 195 (2017).

[24] R. Bruchhaus, D. Pitzer, M. Schreiter, W. Wersing. J. Electroceram. **3**, *2*, 151 (1999).

[25] I.P. Pronin, E.Yu. Kaptelov, A.V. Gol'tsev, V.P. Afanas'ev. Phys. Solid State **45**, *9*, 1768 (2003).

[26] M.V. Staritsyn, M.L. Fedoseev, E.Yu. Kaptelov, S.V. Senkevich, I.P. Pronin. Fiziko-khimicheskiye aspekty izucheniya klasterov, nanostruktur i nanomaterialov. Tver. gos. un-t, Tver **13**, 400 (2021) (in Russian).

[27] D.M. Dolgintsev, E.Yu. Kaptelov, S.V. Senkevich, I.P. Pronin, V.P. Pronin. Phys. Complex Systems **2**, *3*, 101 (2021).

[28] V.A. Volpyas, A.B. Kozyrev. JETP **113**, *1*, 172 (2011).

[29] V.A. Vol'pyas, A.B. Kozyrev, A.V. Tumarkin, D.M. Dolgintsev, V.P. Pronin, E.Yu. Kaptelov, S.V. Senkevich, V.P. Pronin. Phys. Solid State **61**, *7*, 1223 (2019).

[30] C.M. Foster, G.-R. Bai, R. Csencsits, J. Vetrone, R. Jammy, L.A. Wills, E. Carr, J. Amano. J. Appl. Phys. **81**, *5*, 2349 (1997).

[31] T. Oikawa, M. Aratani, H. Funakubo, K. Saito, M. Mizuhira. J. Appl. Phys. **95**, *6*, 3111 (2004).

Translated by Ego Translating